



ORIGINAL ARTICLE

Incomplete radiofrequency ablation provokes colorectal cancer liver metastases through heat shock response by PKC α /Fra-1 pathway

Zhanguo Zhang, Yuxin Zhang, Lei Zhang, Youliang Pei, Yanhui Wu, Huifang Liang, Wanguang Zhang, Bixiang Zhang

Hepatic Surgery Center, Tongji Hospital, Tongji Medical College, Huazhong University of Science and Technology; Hubei Clinical Medicine Research Center for Hepatic Surgery, Wuhan 430030, China

ABSTRACT

Objective: Incomplete radiofrequency ablation (ICR) has been proposed as a major cause of recurrence in the treatment of hepatic metastatic tumors. We tried to determine the mechanisms of this progression in colorectal cancer (CRC) liver metastasis (CRLMs)

Methods: We have established a mouse model of radiofrequency ablation (RFA) therapy to demonstrate increased risk of recurrence of CRLMs with ICR. Here we focused on heat shock-induced CRC malignancy. Sub-lethal heat shock (HS) in CRC cell lines provoked cell growth, invasion, and tumor initiation *in vitro* and *in vivo*.

Results: We found that Fra-1, which lies downstream of PKC α -ERK1/2 signaling, was significantly increased by HS compared with the untreated CRC cells. Silencing Fra-1 reversed the tumor promoting effects of HS. Furthermore, proliferation and tumor initiation inducer *c-Myc*, together with tumor invasion inducer matrix-metalloproteinase 1 (MMP-1) expression were up-regulated by AP-1/Fra-1 induced genes transcription.

Conclusions: Our study demonstrated that ICR generated HS induces CRC malignancy by targeting Fra-1, which could be a potential prognostic marker and a promising therapeutic strategy to prevent disease recurrence after radiofrequency ablation treatment.

KEYWORDS

Radiofrequency ablation; heat shock; colorectal cancer liver metastases; cancer stem cells; recurrence

Introduction

Colorectal cancer (CRC) is the third most commonly diagnosed cancer in males and the second in females, with over 1.8 million new cancer cases and 881,000 deaths estimated to have occurred in 2018^{1,2}. For advanced CRC, the liver is proved to be the first metastatic site. Approximately one-half of patients with CRC will develop hepatic metastases, which are responsible for most of CRC patient deaths^{3,4}. Hepatic resection (HR) is the only curative therapy for CRC patients with hepatic metastases, but it is only suitable for 15%–20% of patients. In the past decade, radiofrequency ablation (RFA) has been developed as an alternative for those patients with unresectable tumors⁵. RFA results in local tissue necrosis by generating a temperature of

> 50°C^{6,7}, yet complete ablation is very difficult to achieve. Both tumor size and localization are the important determining factors for a successful ablation treatment. Tumors larger than 3 cm in diameter have higher risk to get an incomplete ablation^{8,9}. There is a trend of patients obtained a more aggressive cancer phenotype after incomplete RFA treatment.

In addition to the acute induction of heat shock (HS) proteins (HSP27, HSP70, HSP90, HSP60), which protect the cells from the harmful effects of stressful stimuli, HS elicits specific and highly regulated signaling cascades to promote cellular homeostasis¹⁰. The mitogen-activated protein kinases (MAPK) and protein kinase family are both induced by HS stress¹¹. The extracellular signal-regulated kinase (ERK) / MAPK signaling pathway promotes cell proliferation, survival and metastasis and is associated with many oncogenes. In the nucleus ERK induces components of activator protein-1 (AP1) transcription factor complexes, such as *c-Jun* and *c-Fos*. Fra-1 (Fosl1) is a Fos family member that heterodimerises with Jun family members to form the activator protein (AP-1) transcription factor complex.

Correspondence to: Wanguang Zhang and Bixiang Zhang
E-mail: wgzhang@tjh.tjmu.edu.cn and bixiangzhang@163.com
Received October 14, 2018; accepted January 9, 2019.
Available at www.cancerbiomed.org
Copyright © 2019 by Cancer Biology & Medicine

Functionally, Fra-1 expression promotes tumor cell proliferation and initiation, inhibits apoptosis, increases invasion and metastases^{12,13}.

Discrete steps contribute to the biological cascade of metastasis: loss of cellular adhesion, increase of cell motility and invasiveness, intravasation and survival in the circulation, extravasation and colonization of a distant site^{14,15}. Matrix metalloproteinases (MMPs) through the cleaving of the extracellular matrix and allowing cell invasion of the stroma, play a key role in many of these steps. They are divided into collagenases, gelatinases, and stromelysins. There are eight distinct structural classes of MMPs: five are secreted and three belong to membrane-type MMPs (MT-MMPs)¹⁶. Notably, HS was found to induce MMP-1 and MMP-3 expression at the mRNA and protein levels by activating ERK and JNK pathways in primary human skin fibroblasts¹⁷ although it is unclear whether this is true in tumor cells.

Stem cells self-renew, creating daughter cells that retain pluripotency. It is possible to convert a fully differentiated cell into a stem cell by the forced expression of Sox2, Sox9, Oct3/4, c-Myc. Besides iPS phenotype, c-Myc also contributes to cancer stem cell maintenance and cell cycle driven cancer cell proliferation¹⁸. It has been proposed a small proportion of cancer cells within a tumor represent a tumor stem cell population that are endowed with a similar self-renewal capacity^{19,20}. These cells are theoretically critical for the formation of distant metastasis. Tumors with a high proportion of tumor-initiating stem cells (TICs) with the ability to invade stromal matrix would be expected to rapidly metastasize²¹. Here we report that c-Myc transcription is dependent on Fra-1, which is activated by HS.

In this study, we assessed the role of HS stress in the recurrence of CRLMs after RFA treatment. Two strategies were used: *in vivo*, we established a mouse model of RFA therapy. *In vitro* we explored the cellular and molecular events induced by HS on CRC cell lines. We showed that Fra-1 is the main regulator in HS-induced recurrence of CRLMs. These results altogether suggested a malignant inducing role of incomplete radiofrequency ablation (ICR) generated-HS in the progression of metastasis CRC in patients.

Materials and methods

Materials and cell culture

All inhibitors used in this paper were purchased from Tocris (Bristol, UK). Then dissolved in DMSO (Sigma), and stored in aliquots at -20°C before use. CT-26 and SW620 cell lines

were obtained from and authentication (*via* short tandem repeat profiling) by the American Type Culture Collection (2011 and 2010, respectively). Cells used for this study were cryopreserved within 6 months of authentication. CT-26 was cultured in RPMI-1640, SW620 was cultured in DMEM/F12 supplemented with 10% fetal bovine serum (Gibco), 2mM L-Glutamine (Gibco), streptomycin (100 $\mu\text{g}/\text{mL}$) and penicillin (100 U/mL).

Heat treatment

CT-26 and SW620 were grown to 70% confluence, trypsinized and collected into the tubes. A million of cells in 1mL complete media were exposed to HS in a water bath at 37°C or 45°C for 10 min. further culture for 3 days, 5 days and 10 days was done for individual experiments as mentioned.

Gelatin zymography

At day 3 after heating, cells were cultured in serum-free medium with or without inhibitors for 24 h. Conditioned medium was then collected, filtrated with 0.45 μm filter (corning), and concentrated (50 fold) using Amicon centricon-15 concentrators (Millipore). Equal amount of conditioned medium samples were mixed with SDS sample buffer containing 2% SDS without β -mercaptoethanol. Non-boiled samples were loaded to 10% Zymogram (Gelatin) Gel (Novex). After electrophoresis, gels were washed for 30 min at room temperature with gentle agitation in renaturing buffer (2.5% Triton X-100 in H_2O) to remove SDS, followed by washing in equilibrated in developing buffer (50 mM Tris-HCl, pH 7.5, 200 mM NaCl, 5 mM CaCl_2 , 0.02% Brij-35) at room temperature for 30 min. After removing the old developing buffer, the gels were incubated in fresh developing buffer at 37°C overnight. The gels were then stained with Gel staining Blue (Bio-Rad) for 2 h and destained to define signal as clear bands. Gels were photographed using a ChemiDocTM XRS+ System (Bio-Rad).

Animal studies

Four-six weeks aged female BALB/c mice were purchased from the Chinese Academy of Medical Sciences Institute of experimental animals. All experiments involving animals were performed according to the guidelines on laboratory animals of the National Institutes of Health guidelines (NIH publication 96-01, 1996 revision) and were approved by the Institute Research Ethics Committee at the Tongji Medical

College, Huazhong University of Science and Technology (Permit number: SYXK 2010-0057). The CT-26 expressing Luciferase and GFP cells were harvested by trypsinization, washed twice in PBS, then resuspended (5×10^6 cells/mL) in mixture of PBS and growth factor reduced Matrigel in 1 : 1 ratio (BD Biosciences San Jose, CA, USA). One hundred microliter of cells (5×10^5) were injected subcutaneously into the flank of female BALB/c mouse. After 10 days, the tumor was removed and cut into small pieces. $1 \times 1 \times 1$ mm³ tumor masses were adopted for liver xenograft assay. Four-six weeks BALB/c mice were anesthetized using isoflurane and a middle line small incision was made to expose left lobe of liver. Tumor mass was directly implanted into the left lobe of liver below the capsule. The incision was closed with surgical suture (Johnson & Johnson). Ten days later, luciferase activity was monitored using Xenogen IVIS Imaging System (Caliper Life Sciences, Waltham, MA, USA). Mice with similar bioluminescence mice were used for proceeding RFA surgery. A little bit left aside by the middle line incision (in case of broken the ankyloenteron intestine) was made in order to expose the tumor burdened left liver lobe. The RFA needle (StarBurst[®] Radiofrequency Ablation System) was inserted into the middle of the tumor for 2 min of 53°C heating for CR group and 1 minute for ICR group. In sham group, the incisions were only made and then sutured without performing RFA or HS. Mice were imaged for luciferase activity every week. We considered the endpoint of the experiment when ICR group mice turning sick (4 weeks after RFA surgery). Organs with tumors were collected for pathology experiment. The same experiment was repeated for survival study. The value of qualified signal was showed in **Supplementary Table S1**.

Four-weeks-old female nude mice were used for the subcutaneous tumor xenograft. The assay runs the same way as mentioned. When palpable tumors were formed, they were measured by digital scale every three days. Tumor volume was estimated using the following formula: volume = $\pi \times \text{width}^2 \times \text{length} / 6$. When the ending point was reached, mice were sacrificed and tumors were harvested for further experiments.

Real-time RT-PCR

The expression of mRNA for *mmp1a*, *mmp2*, *mmp3*, *mmp7*, *mmp9*, *mmp14* and *mmp20* were examined by real-time RT-PCR using the Taqman Rox Mix (Roche, Basel, Switzerland) on 7500 system (ABI). Data were acquired using an ABI PRISM 7500 system (Applied Biosystems). Each reaction was performed in triplicate. Results were normalized

to human or mouse *Gapdh* mRNA. All the primers used in this experiment were purchased from Applied Biosystems. The primer catalog numbers were listed in **Supplementary Table S2**.

Colosphere assay

Colosphere assays were performed as described previously^{22,23}. One thousand of cells were properly filtered and suspended in serum free DMEM/F12 medium (Gibco, Gran Island, NY, USA) supplemented with 20 ng/ml epidermal growth factor (EGF, Invitrogen), 20 ng/mL basic fibroblast growth factor (bFGF, Invitrogen), 1 : 50 B27 supplement (Gibco), 0.2% cell cultured grade BSA (Sigma, St. Louis, MO, USA), 100 units/ml penicillin (Gibco), and 100 μ g/mL streptomycin (Gibco) at a density of 3,000 cells per well in ultralow attachment 24-well plates (Corning, MA, USA). After 4 days (CT-26) or 7 days (SW620) culture, pictures were captured by microscopy, the number and size of colospheres was observed using GelCount[™] machine (Oxford Optronix, UK).

Cell invasion assay

For cell invasion assay, transwell chamber (pore size 8 μ m) with pre-coated matrigel membrane filter (Corning) was used. 5×10^4 CT-26 cells in RPMI-1640 medium or 1×10^5 SW620 cells in the DMEM/F12 medium containing 0.2% BSA were layered in the upper chamber, medium containing 10% FBS, DMSO (1/1,000 v/v) or U0126 (10 μ M) or Gö6976 (500 nM) was applied to the lower chamber. The chamber was incubated for 24 h at 37°C. Then, after the upper surface of the filters was removed, the invaded cells were fixed with 4% paraformaldehyde solution and stained with 0.1% crystal violet. The number of invaded cells was quantified by counting the cell number at 10 random fields.

Western blot

Cells after treatment or mice xenograft tumors were lysed using RIPA buffer (50 mM Tris PH 7.4, 150 mM NaCl, 0.1% SDS, 1% Triton X-100, 0.5% sodium deoxycholate, 10% Glycerol, 1 mM EGTA, 4 mM EDTA) with phosstop (Roche) and proteinase inhibitor (Roche). The protein concentrations were measured by BCA Protein Assay kit (Pierce, IL, USA), and then Western blot analysis was performed as previously described. The antibodies we used were listed in **Supplementary Table S3**.

Apoptosis assay

Apoptosis was performed using Alexa Fluor 488-Annexin V/PI (Invitrogen, Carlsbad, CA, USA). Forty-eight hours after HS, cells including suspension and adherence cells were collected and stained with Annexin V and PI following the manufacturer's protocol. Samples were analyzed by flow cytometry using a BD LSR II flow cytometer (BD Biosciences, San Jose, CA, USA) and results were evaluated using FlowJo analysis software (Tree Star, Inc., Ashland, OR, USA). Annexin V positive staining cells were regarded as apoptotic cells.

Proliferation assay

Proliferation assay was measured by Brdu incorporation assay. At day 3 after heating treatment, cells were trypsinized and plated on glass coverslips in 24 wells plates. After another 24 h incubation with or without inhibitors, culture medium was replaced with Brdu incorporation medium for 1 hour followed by 70% ethanol/glycine fixation for 1 h in -20°C . For Brdu staining, coverslips were incubated with mouse anti-Brdu antibody (Roche) overnight at 4°C . After that, the coverslips were washed and then incubated with Alex Flour 594-conjugated anti-mouse IgG (Invitrogen). For actin cytoskeleton staining, coverslips were incubated with FITC-coupled phalloidin for 30 min. Nuclei were labeled with DAPI. Cells were examined with a Leica DMP A microscope. The numbers of Brdu+ cells were quantified by counting cells at 10 random fields.

Knockdown of the target genes by siRNAs

Smartpool siRNAs for Fra-1, c-Myc and control siRNA were purchased from GE (Pittsburgh, PA, USA). After grown to 80%–90% confluence, the CT-26 cells were transiently transfected using Transfect Reagent1 (Dhamacon) with siRNA pools (Dhamacon). Six hours later, the cells were cultured in complete medium for 48 h (gene expression analysis) and 72 h (protein level analysis). Then the cells were harvested and the assays were performed including real-time RT-PCR and Western blot.

Luciferase reporter gene assays

Cells cultured on 24-well plates (0.5×10^6 cells/well) were transfected using Lipofectamine 2000. Firefly luciferase and Renilla luciferase activities were evaluated using commercial

assay kits (Promega). Recordings were performed using an Infinite M200 microplate reader. Transcriptional activity was determined as luciferase activity normalized to Renilla luciferase activity and compared with controls.

PKC kinase activity assay

Protein kinase C activity was performed according to instructions of manufacturer (Enzo Life Science, #ADI-EKS-420A), which is based on a solid phase enzyme linked immuno-absorbent assay (ELISA).

Statistical analysis

All of the results were showed as mean \pm SD, unless otherwise stated. All experiments were repeated at least three times. The statistical significance of experimental groups and controls was determined by two-sided Student's *t* test. Comparisons between three or more groups were done with ANOVA. In all cases, findings were considered statistically significant if *P* value was < 0.05 (* represents $P < 0.05$, ** represents $P < 0.01$ and *** represents $P < 0.001$).

Results

Effect of HS on colorectal cancer metastasis in an experimental mouse model resembling incomplete RFA treatment in patients

To elucidate whether the incomplete RFA-induced HS can stimulate aggressive tumor recurrence, we used the stably pFUW-luciferase-T2A-GFP-transfected CT-26 colon adenocarcinoma cells for tracking metastatic tumor cells *in vivo* (Figure 1A). In this experiment, pFUW-Luciferase-T2A-GFP-expressing CT-26 cells were first subcutaneously injected into BALB/c mice. As tumors grew to 1 cm^3 , they were resected into small pieces and orthotopically transplanted into the BALB/c mice through liver surgery. Ten days after transplantation, fluorescence was assayed to determine the tumors formed within liver. Only mice with the similar fluorescent intensity of tumors were chose and further given RFA treatment (the process was summarized in Figure 1B). Four weeks later, we observed that in sham group, the orthotopically transplanted CT-26 GFP cells developed high fluorescent signal mainly in mice liver, while there was no or relatively weak fluorescent signal detected in the CR-treated group. In contrast, mice from ICR-treated group developed stronger fluorescent signal not only in liver,

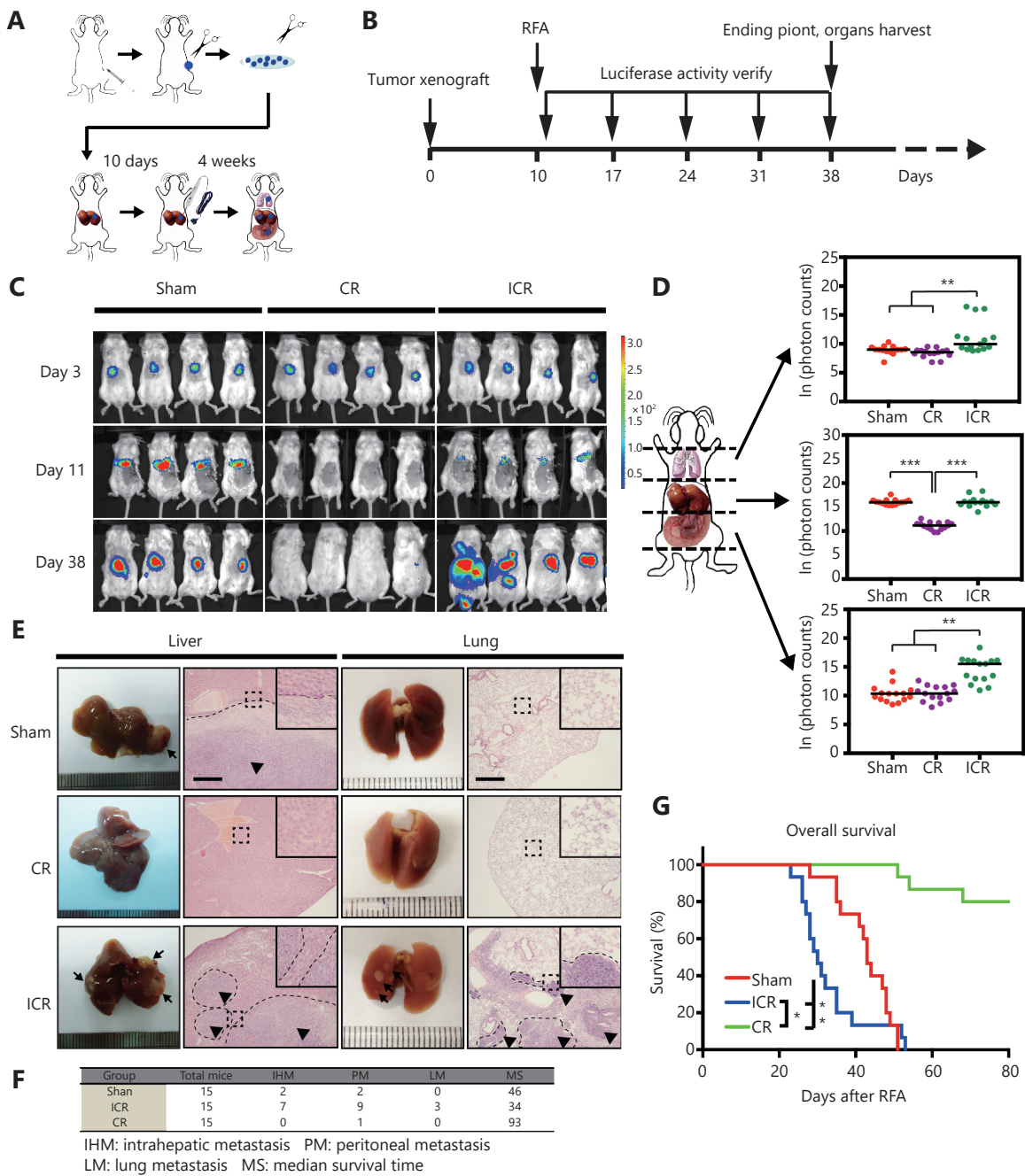


Figure 1 Incomplete ablation induces CRLMs recurrence *in vivo*. (A, B) Schematic outline of the xenograft model used in our study. Tumor pieces of equal volume (1 mm^3) from the CT-26 subcutaneous xenograft tumor were transplanted into the livers of BALB/c mice. Ten days after orthotopic implantation, RFA was performed. Four weeks later, mice were killed and then their liver and lung tissues were harvested and analysed by histology or gene and protein expression. (C) Representative luminescence images and paired organs (lung and liver) from each group. ICR, incomplete RFA; CR, complete RFA. (D) Luminescence was determined in three positions (lung/upper part, liver/middle part and PM/lower part) by the schematic shown (left). The base e logarithm of the luminescence value from three groups was shown in the graft (right). P values were determined by ANOVA test. * $P < 0.05$, ** $P < 0.01$. (E) Representative lung and liver H&E stained histology samples ($100 \times$). Arrows indicate metastatic lesions. (F) Information about three groups was listed. IHM, intrahepatic metastasis; PM, peritoneal metastasis; LM, lung metastasis; MS, median survival time. (G) Kaplan-Meier overall survival curve in the xenograft mouse model suffered with RFA treatment ($n = 15$ in each group). P values were determined by log-rank test. * $P < 0.05$, ** $P < 0.01$.

but also the nearby area of abdomen and lungs, suggesting the local and distant metastasis of tumor (Figure 1C and 1D). Analysis of tumor growth pattern and location revealed that mice in sham group displayed single tumor foci in liver, CR group had no tumor growth and the liver regenerated successfully in response to RFA treatment. In contrast, treatment with ICR caused a generally increased growth of orthotopic tumors, but also changed the pattern of tumor cell growth to multicellular foci *via* spreading to the intrahepatic, peritoneal, and lung areas (Figure 1C, 1E and Supplementary Figure S1A). Furthermore, tumor cells were found in the bloody ascites after metastatic tumor destroyed the peritoneal membrane and spread inside the peritoneal cavity (Supplementary Figure S1A and S1B). Histopathological analysis confirmed the severe damage caused by local and distant metastasis of CT-26 cell in ICR group (Figure 1E). Consistently, mice in the ICR group showed a shorter survival than those in the sham group and CR group (Figure 1F and 1G). Therefore, using orthotopic implantation of Luciferase-T2A-GFP-expressing CT-26 colorectal cancer cells, we confirmed that HS induced by the incomplete RFA treatment led to a much aggressive liver metastasis in the surgery animal model.

HS stress enhances CRC cell proliferation *in vitro*

To investigate the effect of HS on CRC cell lines, we treated two metastatic cell lines CT-26 and SW620 with the different temperature range at 37°C, 42°C, 45°C, 48°C, 50°C and 55°C for 10 min. 48 hours later, cell viability was measured by Annexin V and PI staining. As shown in Figure 2A, the temperature that induced CT-26 apoptosis was 48°C and no survival cells were found upon 50°C and 55°C treatment. The similar result was observed in SW620 cells (Figure 2A). We further evaluated the effect of HS on cellular proliferation using Brdu incorporation assay. The temperatures that induced cell proliferation were 45°C and 48°C, determined by Brdu positive index (BPI, Brdu+ cells/total cells) both in CT-26 cells (Figure 2B) and SW620 cells (Figure 2C). Consistently, the level of cell cycle-related proteins was altered substantially in response to 48°C treatment, including the up-regulation of cyclin D1 at day 10, cyclin D2 at day 5, and Rb phosphorylation at day 5 in CT-26 cells. In contrast, the cyclin-dependent kinase inhibitor 1A (p21) and inhibitor 1B (p27^{kip1}) were down-regulated responding to 45°C and 48°C HS treatment. Taken together, HS stimuli induced CRC cell proliferation in a cell-cycle dependent manner *in vitro* (Supplementary Figure S2).

HS stress enhances the self-renewal ability of CRC cells *in vitro*

Cancer cells need to acquire some of the characteristics of stem cells to survive. These include immortality, the ability to self-renew and the capacity to produce progenitors that differentiate into other cell types²⁴⁻²⁶. To determine if HS promotes CRC cell self-renewal and differentiation into a CSC-like cell type, we performed the sphere-forming assay by growing either CT-26 (Figure 3A-3C) or SW620 (Supplementary Figure S3A-S3C) with sphere-promoting conditions. Cells undergoing 45°C or 48°C stress displayed a higher sphere-forming efficiency than untreated and 42°C treated cells, suggesting that the generation of stem-like cells depends on cellular stress induced by increased temperatures.

HS stress enhances invasion of CRC cells *in vitro* as well as the MMP-1 expression

To further investigate that HS-induced CSC-like cell type acquires an invasive phenotype, which contributes to CRC metastasis and progression, we performed the *in vitro* invasion assay. It appeared that HS treatment at 45°C or 48°C increased invasion efficiency of CT-26 cells up to 70% by day 5 compared with untreated and 42°C treated cells (Figure 3D left panel and supplementary Figure S3D upper panel). Similar results were observed in SW620 cells, with a 25% and 65% increase of invasion at 45°C or 48°C, respectively (Figure 3D right panel and Supplementary Figure S3D lower panel).

Expression of various MMPs has been found to be up-regulated in many different human cancers and correlates with advanced stage, invasive and metastatic properties and, in general, poor prognosis. In particular, HS stress has been shown to induce MMP transcription¹⁷. We next measured the mRNA levels of several MMPs in CT-26 cells 3 days after HS treatment, including collagenases (MMP1), Gelatinases (MMP2 and MMP9), Stromelysins (MMP3), membrane-type MMPs (MMP14), Matrilysin (MMP7), and Enamelysin (MMP20). As shown in Supplementary Figure S4A, we detected the up-regulation of MMP-1a upon 45°C and 48°C treatment, but not other MMPs in CT-26 cells. As control, representative MMPs expression level was confirmed by western blot assay or Gelatin zymography assay, only MMP1 was up-regulated by HS both in CT-26 and SW620 cells (Figure 3E). Taken together, these data showed that HS induced the expression of MMP-1 in CRC, but not other MMPs.

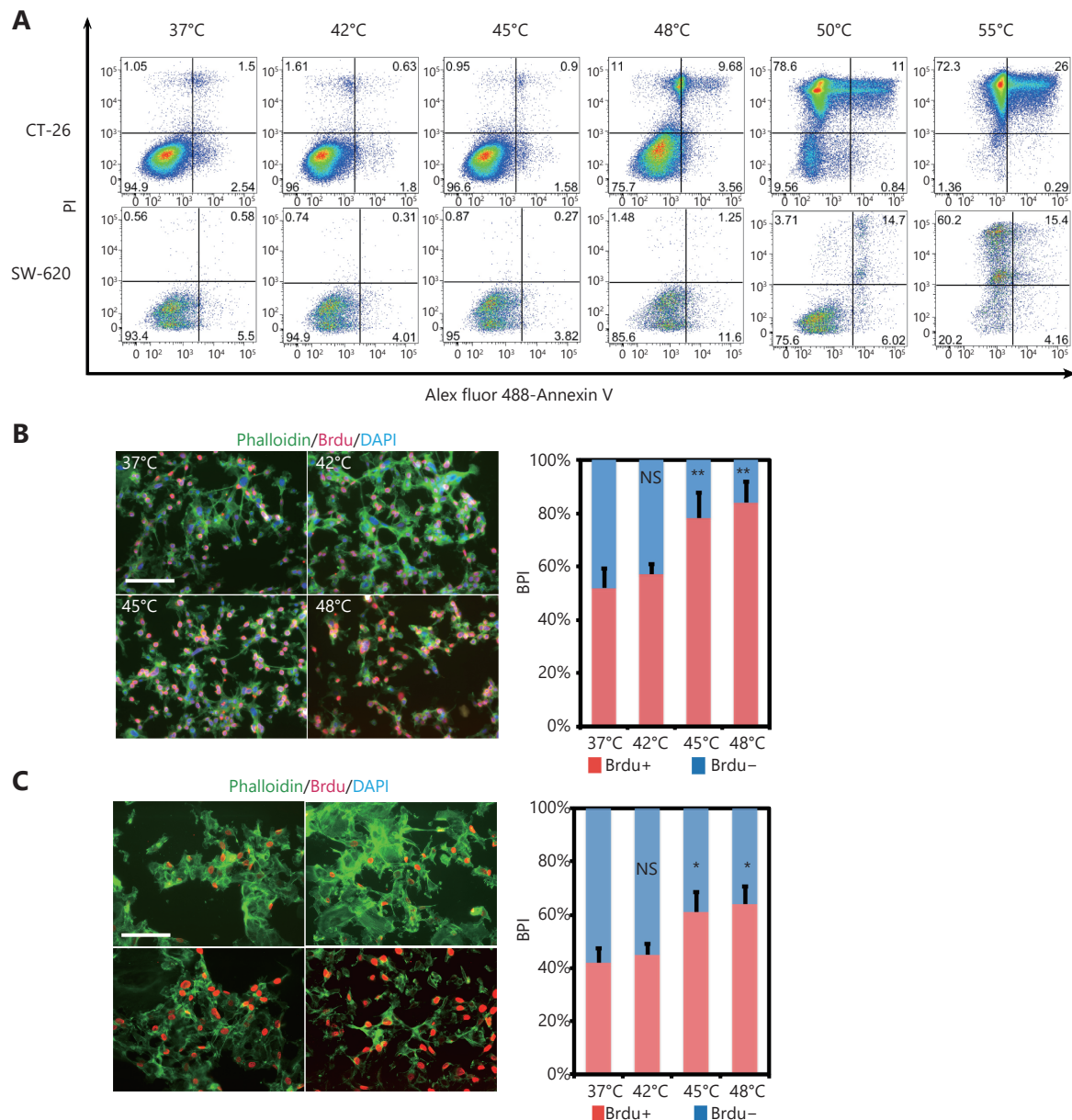


Figure 2 HS promotes CRC proliferation *in vitro*. (A) CRC cell lines were exposed to HS at the temperatures indicated for 10 minutes, followed by cell culture in complete medium for 48 hours. Cells were double labeled with Alexa fluor 488-Annexin V and PI, then analyzed by FACS. The results shown are representative from three independent experiments. (B, C) Proliferation of CT-26 and SW620 cells treated by different temperatures' HS as measured by BrdU incorporation. BrdU incorporation was detected by immunofluorescent staining (B, C). The percentage of BrdU positive cells (BPI) in CT-26 cells (B) and SW620 cells (C) were quantitatively measured. Red, BrdU; Green, phalloidin; Blue, DAPI (200 \times). *P* values were determined by one-way ANOVA test. * *P* < 0.05, ** *P* < 0.01 (*n* = 3).

HS induces PKC α -(ERK1/2)-Fra-1 cascade in a c-Met independent manner

Previous studies indicate that HS stress-mediated signaling involves MAPK and PKC pathways^{11,27}. We confirmed the phosphorylation of PKC α and ERK1/2 in CT-26 cells after

HS and its activation was sustained for at least 10 days, as shown in **Figure 4A**. Fra-1, a downstream target of PKC α and ERK, a key factor in the formation of pluripotent stem cell, were observed highly phosphorylated upon HS. Furthermore, the PKC activity was up-regulated by HS in CT-26 and SW620 cells (**Figure 4B**). In addition, a stem cell

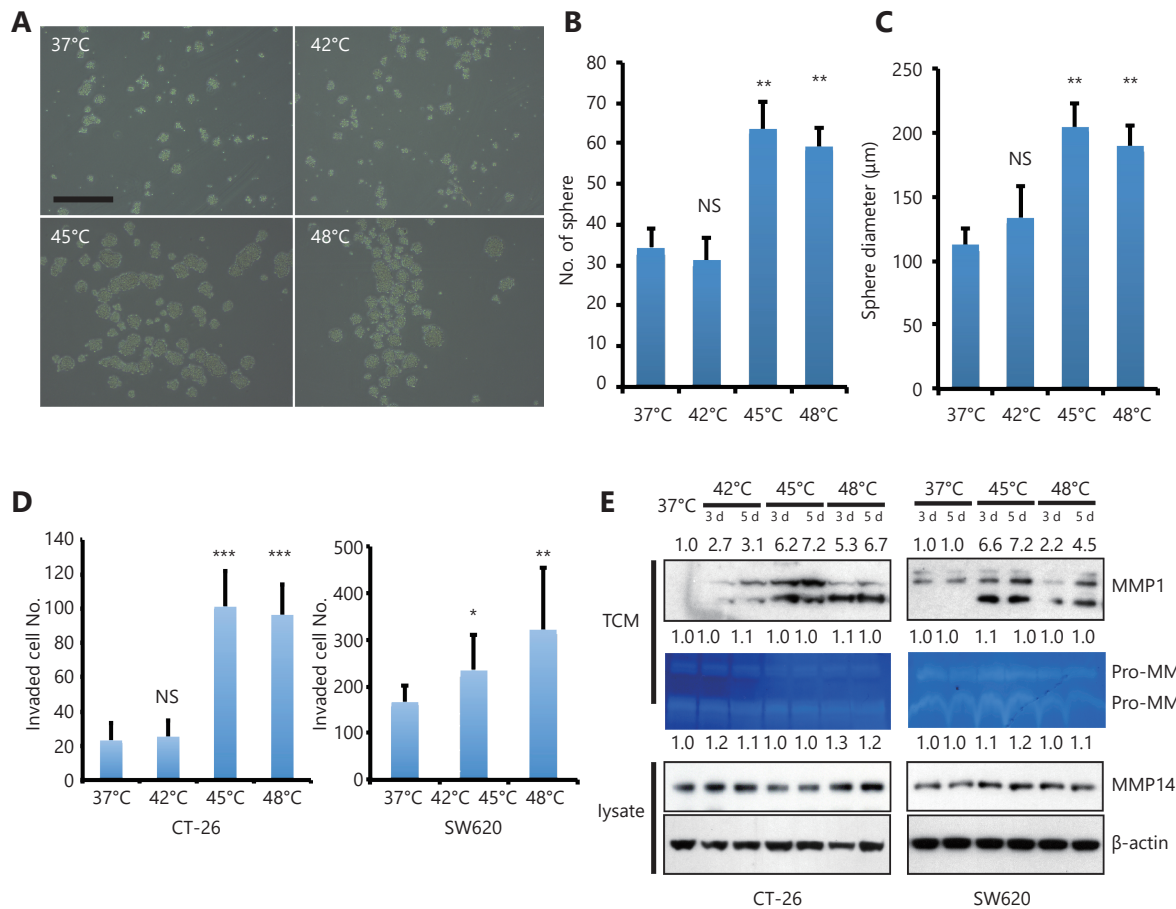


Figure 3 HS promotes tumor-initiating cell traits and invasion capacity. (A) Phase-contrast pictures of tumor spheres formed by HS treated CT-26 cells, grown in serum-free sphere medium on ultra-low attachment surface plates (scale bar, 200 μm). (B, C) Quantification of tumor spheres formed by CT-26 cells. The mean number of spheres per 5,000 cells (B) and the mean diameter of spheres (C) are calculated in triplicate samples. (D) Matrigel pre-coated Transwell assays were performed to examine the invasion ability of CT-26 and SW620 cell 3 days after HS treatment, CT-26 (24hrs), SW-620 (36hrs). Western blot assay was performed with cell lysate and Tissue culture Condition Media (TCM). Gelatin zymography assay was performed with TCM. The quantification value was labeled above the bands. *P* values were determined by ANOVA test. * *P* < 0.05, ** *P* < 0.01. All data were from three independent experiments.

pluripotency-associated molecule, c-Myc was up-regulated by HS, whereas down-regulated in the presence of Gö6976, an specific inhibitor of PKCα; U0126, an inhibitor of ERK signaling or by the silencing of Fra-1 using siRNA (Figure 4A and 4C). Furthermore, the opposite results were obtained when Fra-1 was over expressed (Supplementary Figure S4B.) The results therefore suggested that HS-mediated PKCα-ERK-Fra-1 maybe required for CRC to gain poorly differentiated feature, similar to the characterized self-renewal or stemness property of CSC in carcinogenesis.

Hepatocyte growth factor (HGF)/c-Met stimulation is known to activate ERK1/2. We confirmed this in CT-26 cell line with HGF stimulation in the presence or absence of a c-Met inhibitor. Cellular stress, including hypoxia, can induce HGF receptor c-Met expression, contributing to increase the

metastatic potential of tumor cells^{28,29}. We next tested if c-Met is involved in HS-induced ERK activation. However, we did not find any difference in the phosphorylation status of c-Met in CT-26 cells after HS treatment. Furthermore, HS-induced ERK1/2-Fra-1 activation was not influenced by c-Met inhibition (Supplementary Figure S5A-S5C). The result thus suggested that activation of Fra-1 by HS was independent of c-Met.

Role of PKCα-(ERK1/2)-Fra-1 cascade in HS-induced cancer progression

To further understand the molecular mechanism of which pathway is involved in HS-induced CRC self-renewal, we treated the pre-heated CT-26 cells with various kinase

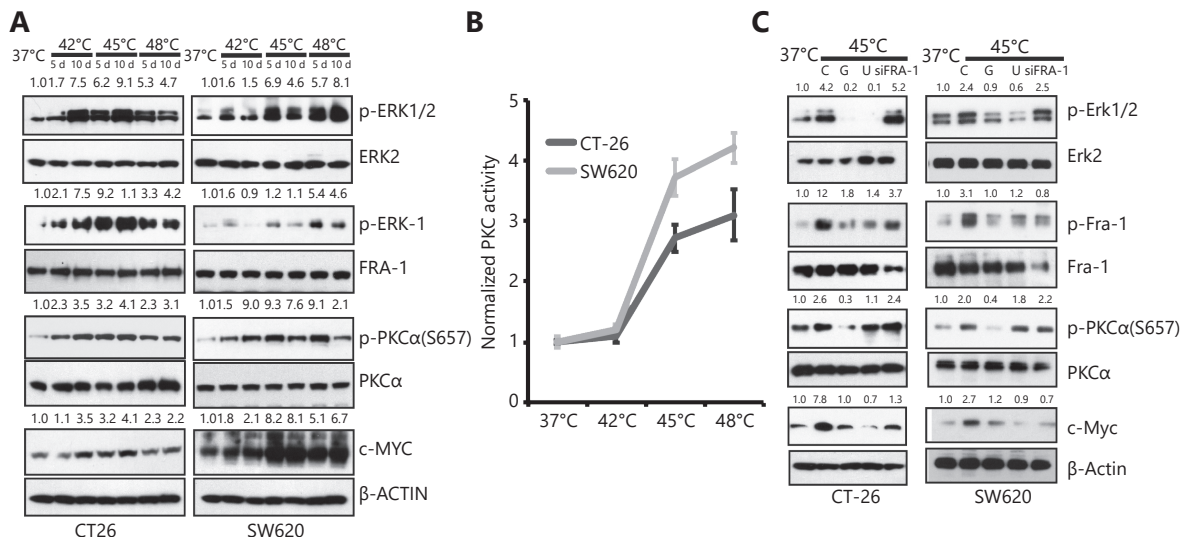


Figure 4 HS activates PKC α -ERK1/2-FRA-1 cascade. (A) Western blot measurement of ERK1/2, FRA-1 and PKC α phosphorylation in HS-treated CRC cells. (B) PKC activity measurement of CT-26 and SW620 cells after HS treatment for 5 days. (C) Western blot analysis of p-ERK1/2, p-FRA-1 and p-PKC α expression in control, HS-treated CT-26 and SW620 cells in the presence or absence of U0126, Gö6976 or FRA-1 siRNA. C: control, G: Gö6976, U: U0126. The quantification value was labeled above the bands. All data were from three independent experiments.

inhibitors. Among them, we found that MEK inhibitor U0126, PKC α inhibitor Gö6976 and c-Myc inhibitor 10058-F4, block the sphere forming ability after HS (Figure 5B and Supplementary Figure S6A-S6B). Fra-1 knock down and Myc knock down also abolished the ability of CT-26 cells to form colospheres (Figure 5B).

To determine whether ERK1/2-Fra-1 is involved in HS-induced CRC cell proliferation, Brdu labeling assay was performed, revealing that Gö6976, U0126, Fra-1 siRNA and c-Myc siRNA could inhibit the HS-induced CT-26 cell proliferation (Figure 5A). Similarly, Gö6976, U0126 or Fra-1 siRNA was applied to evaluate whether PKC α -(ERK1/2)-Fra-1 plays roles in HS-induced MMP-1 expression and CRC cell invasion. We observed the increased number of invasion cells and the up-regulation MMP-1 expression in both CT-26 and SW620 cells after HS treatment and the effects were remarkably suppressed by Gö6976, U0126, Fra-1 siRNAs and MMP-1 siRNAs (Figure 5D and 5E). The result suggested that Fra-1 was a key down-stream activator of PKC α /ERK to regulate MMP-1 expression and controlled the metastatic property of CRC.

Fra-1 regulates c-Myc and MMP-1 transcription by binding their AP-1 promoter

To determine whether the HS-mediated induction of c-Myc and MMP-1 transcription is AP-1 dependent and occurs

directly through the AP-1 binding sites present in the promoters, mutant reporters of the AP-1 binding sites were created. CT-26 and SW620 cells were transfected with one of the reporter constructs and 48 h later were lysed for luciferase reporter assay. In CT-26 and SW620, mutation of the proximal AP-1 binding sites in c-Myc gene promoter decreased its activity to at least 2-fold, which compared with the wild type group ($P < 0.001$) (Figure 5C). Similar effects were observed when the cells were transfected with the MMP-1 promoter constructed luciferase reporter vector. And this activation was significantly reduced when the proximal AP-1 binding site was mutated (Figure 5F). Together, these data demonstrate that HS-induced c-Myc and MMP-1 transcription in colon cancer is mediated by the AP-1/Fra-1 transcription factor.

HS induces larger tumors *in vivo*

To evaluate how the HS induces tumor growth *in vivo*, we subcutaneously injected mice with HS pre-treated CT-26 cells. Tumors formed 5 days after xenograft were larger from 45°C and 48°C pre-treated CT-26 cells (Figure 6A and 6B), compared to those formed from 37°C and 42°C treated cells. Histological analysis showed no difference of tumor cell morphology among the four groups (Figure 6C). Analysis of tumors taken from the 45°C and 48°C treated groups demonstrated a higher levels of proliferation by Ki-67

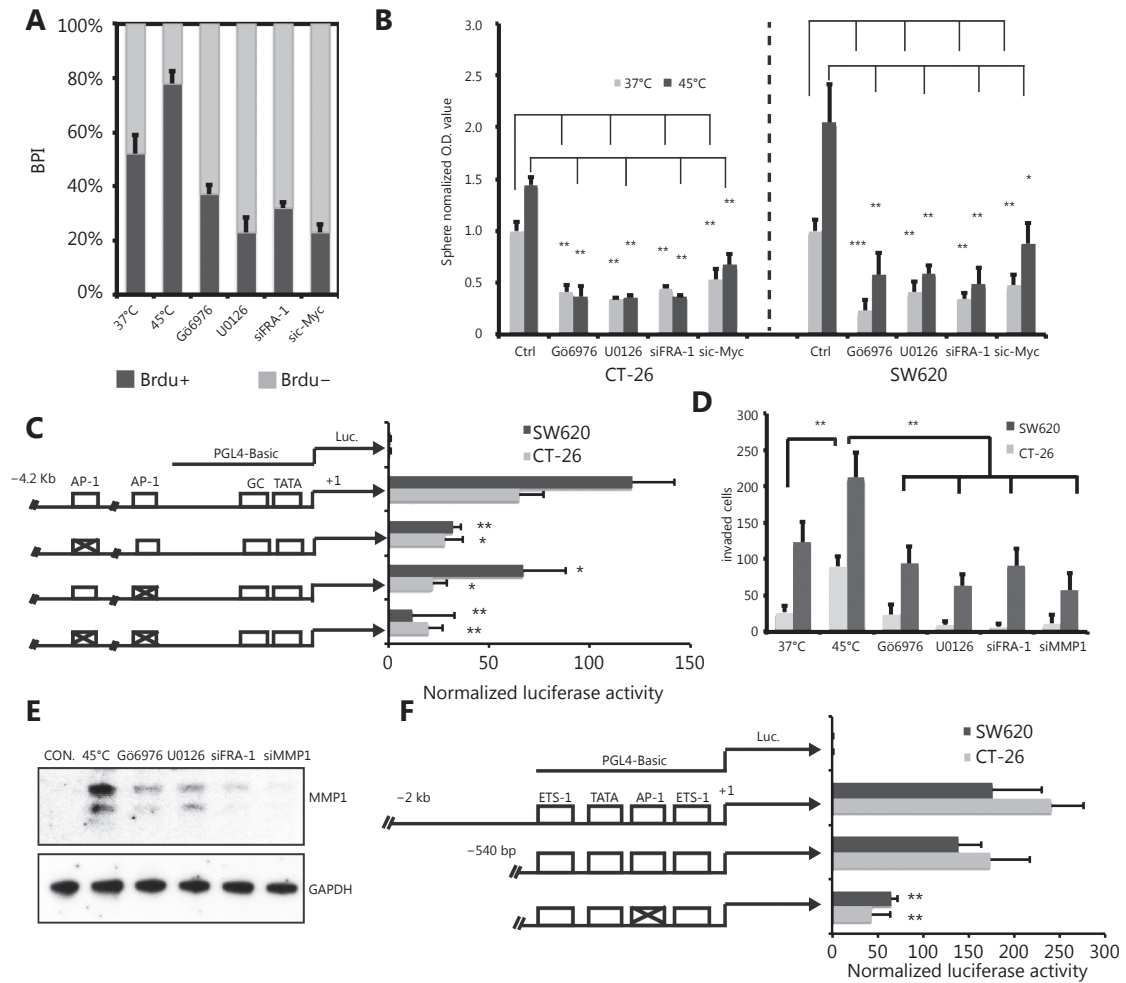


Figure 5 Inhibition of PKCa-ERK1/2-FRA-1 cascade abolished the HS induced malignant effects. (A) BrdU incorporation was detected by immunofluorescent staining. The percentage of BrdU positive cells (BPI) in CT-26 cells were quantitatively measured. (B) Sphere-forming assay of in control and HS-treated CT-26 and SW620 cells in the presence or absence of Gö6976 (300 nM), U0126 (5 µM), Fra-1 siRNA or c-Myc siRNA. Quantification of the spheres by MTT assay. (C) Luciferase reporter assay of c-Myc gene in CT-26 and SW620 cells with or without AP-1 promoter dysfunctional mutation. (D) Matrigel pre-coated Transwell assays were performed to examine the invasion ability of CT-26 and SW620 cells 3 days after HS treatment, in the presence or absence of Gö6976 (300 nM), U0126 (5 µM), Fra-1 siRNA or c-Myc siRNA. (E) Western blot analysis of MMP-1 expression in control and HS-treated CT-26 cells in the presence or absence of inhibitors or siRNAs. The quantification value was labeled above the bands. (F) Luciferase reporter assay of MMP-1 gene with or without AP-1 promoter dysfunctional mutation. *P* values were determined by two-sided Student's *t* or ANOVA test. **P* < 0.05, ***P* < 0.01. All data were from three independent experiments.

staining than in controls, whereas there was no distinguishable difference in cleaved-Caspase 3 expression (Figure 6C and 6D). Taken together, our *in vivo* data confirmed that HS results in forming larger tumors.

Discussion

RFA treatment has been widely used in CRC patients with liver metastases that can not be resected using conventional

surgery³⁰. Despite the short-term success evaluated by the health-related quality of life (HRQL), the therapy is marred by a high rate of local recurrence^{31,32}. The incidence of new hepatic metastases within one year after RFA varies between 44% and 50%, compared to using surgical approaches (12%) or using a laparoscopic approach (47%)^{33,34}. That is linked to incomplete cancer cells depletion³⁵. To date, most studies have focused on hypoxia related recurrence after ICR. In this study, we demonstrated that HS stress is another critical

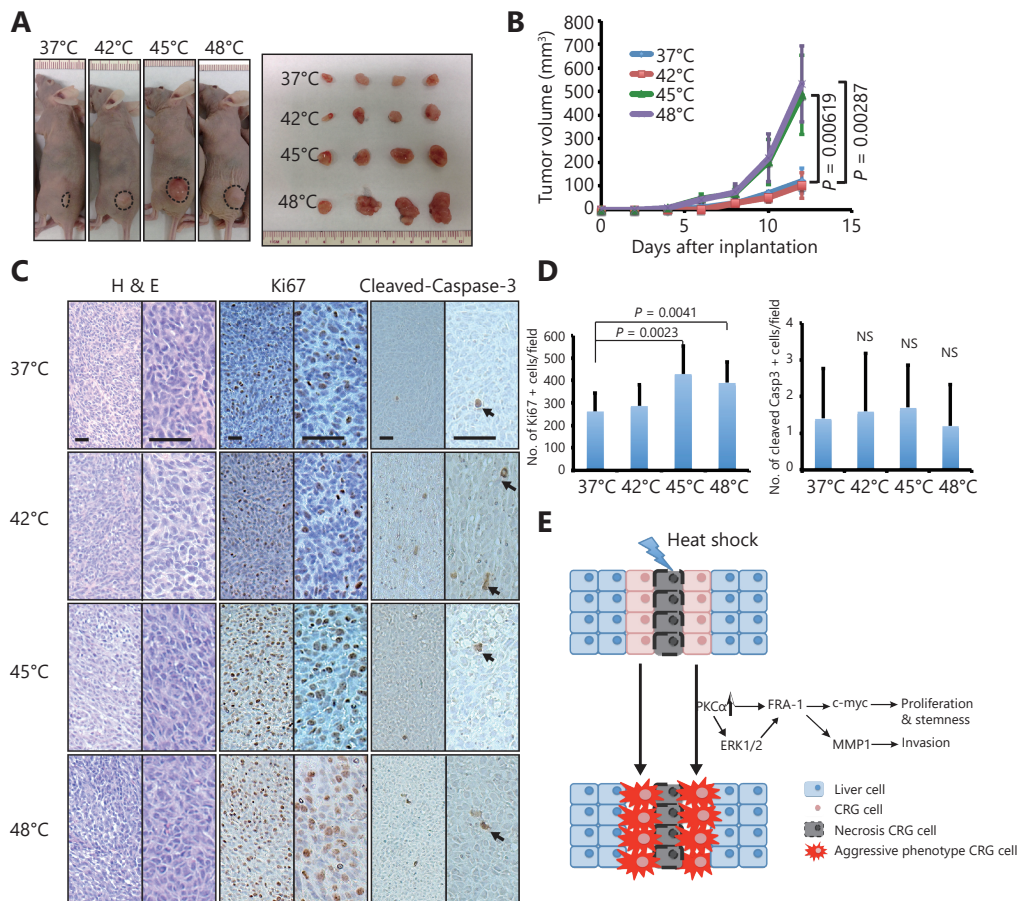


Figure 6 HS enhanced tumorigenesis in a xenograft model. (A) Flank tumors were established in BALB/c nu/nu female mice ($n = 4$ per group) as described in materials and methods. Mice were killed at day 12 after flank injection. Representative tumors were showed. The 45°C and 48°C preheated CT-26 cells resulted in a dramatic rise of tumor weight. (B) Growth curves of xenograft tumors after the injection of pre-treated and untreated cells in mice ($P < 0.01$). (C) Representative hematoxylin and eosin (HE)-staining and IHC staining (Ki67, cleaved-caspase3) images of xenograft tumors harvested from mice that received subcutaneous injection of treated and untreated CT-26 cells. (Magnification: left half is 100 \times , right half part is 200 \times) (D) The numbers of Ki67+ and cleaved-caspase-3+ cells were counted and analyzed with unpaired Student's t -test. (E) Schematic graphs showed HS induced proliferation, invasion and stemness pluripotency related cascade. All data were from three independent experiments.

factor in CRLMs by enhancing proliferation, invasion and metastasis of cancer cells.

To examine the effects of RFA on cancer treatment, previous study has used sublethal heat treatment to skew hepatocellular carcinoma (HCC) cells and colon cancer cells towards epithelial-mesenchymal transition (EMT) and transformed them to a progenitor-like, highly proliferative cellular phenotype *in vitro* and *in vivo*³⁶⁻³⁸. However, it is suggested that this approach could not entirely resemble the effect of ICR in clinical setting^{36,39}. In this study, we established a mouse model through orthotopically inoculating with the luciferase-T2A-GFP stably transfected CT-26 CRC cells to visualize liver metastasis and to accurately represent the *in vivo* process of RFA treatment

(Figure 1). Our data suggest that RFA-mediated HS stress promotes orthotopic cancer growth and induces the emergence of hepatically seeded CRCs into liver metastases.

To understand the underlying molecular mechanisms, we subsequently found that HS stress induced CRC cell proliferation, which was identified by Brdu incorporation assay (Figure 2). Consistent with this, the expression of a number of cell cycle-related proteins by HS, including p-Rb, CyclinD1, CyclinD2, CDK2, p27 and p21 were found altered. The effect of HS on cancer cell proliferation was further confirmed *in vivo* and we observed the cells pre-exposed to 45°C and 48°C induced a higher tumor growth after xenograft, compared to control (Figure 6). We next showed that the PKC α , ERK1/2, and their downstream target, Fra-1

phosphorylation level were enhanced by HS stress (**Figure 4**). Notably, some of the CSC related pluripotent molecules were also up-regulated with the similar pattern as the phosphorylated PKC α , ERK1/2 and Fra-1 upon HS. Furthermore, we found that HS-mediated high sphere forming of CRCs was abolished using PKC α inhibitor Gö6976, MEK inhibitor U0126, Fra-1 siRNA and c-Myc siRNA (**Figure 5** and **Supplementary Figure S6**). Given to accumulating evidences support the idea that malignancies originate from a small fraction of cancer cells that show self-renewal and multi- or pluripotency⁴⁰⁻⁴², our data suggest HS-induced PKC α -(ERK1/2)-Fra-1 signaling pathways may promote proliferation of CSC-like cell for cancer-initiating process and sustaining CRC growth by promoting transcription of c-Myc.

Despite that cancer cells are capable of extensive proliferation, their invasive characteristic also contributes to carcinogenesis. Cancer invasion is supported by the secreted MMPs from different cell types. Their increased enzymatic activity leads to extensive stromal degradation and damage within the epithelial basement membrane (EBM), which facilitates cancer cell release and spread^{43,44}. Therefore, MMPs are positive regulators of cancer invasion and metastasis¹⁶. In this study, we investigated the effects of HS on the expressions of MMPs in CRC cells. Our results showed that HS-induced expression of MMP-1, but not those of MMP-2, MMP-9 and MMP-14. Previous data has indicated that HS rapidly activates all three MAPKs, including ERK1/2, JNK, and p38 in various cancers, among which the ERK1/2 activation was the most significant. However, the downstream pathway of HS-induced ERK1/2 signaling is unknown. In this study, inhibition of PKC α , ERK1/2 and their downstream molecular Fra-1 resulted in the suppression of HS-induced MMP-1 expression, suggesting that HS induces MMP-1 expression through PKC α -(ERK1/2)-Fra-1 cascade. Fra-1 is a member of the c-Fos family member of transcription factor. MMP-1 expression has been shown to be dependent on the activator protein 1 (AP-1) transcription factor, which consists of either homodimeric or heterodimeric complexes formed by c-Jun and c-Fos family members. The ERK pathway is known to contribute to the expressions of these AP-1 transcription factors. It is highly likely that HS-induced activation of the PKC α -ERK1/2 pathway increases Fra-1 associated AP-1 activity, thereby regulating MMP-1 expression.

As the downstream effector of PKC α -ERK1/2, the AP-1 component Fra-1 is found up-regulated to facilitate CRC migration¹². In our studies, proof of the concept for the key role played by Fra-1 in this process responding to HS was

analyzed by specific knockdown of Fra-1 with siRNA, which resulted in a marked suppression of CRC cell invasion *via* a matrigel invasion assay (**Figure 5**). Based on the current view on the importance of stress-activated MAPKs in the regulation of MMP expression, it could be assumed that activation of Fra-1 is responsible for maximal activation of MMP-1 expression in HS stress condition present in CRC and that is not only required for the invasive cancer cells and stromal cells at the invading edge, but also important for survival of cancer cells by acquiring stem-like properties. It is generally agreed that, like all stem cells, the cancer sphere-forming cells are capable of proliferation, self-renewal and possess higher tumorigenicity. We thus gave the CRC cell lines the sphere culture for enriching stem cells, a method which relies on their property of anchorage independent growth (**Figure 3** and **Supplementary Figure S3**). We found that HS promoted the sphere-forming ability of CT-26 and SW620 cells for their stemness characteristics. Inhibition of PKC α , ERK phosphorylation or transfection with Fra-1 siRNA suppressed the anchorage-independent growth in sphere media, as well as the expression of cancer stemness-related transcription factors c-Myc. It will be of great interest to determine whether inhibition of this pathway could serve as a therapeutic target to specifically prevent CRC stem cell activity and the subsequent liver metastatic property.

Conclusions

Although RFA is currently an important and widely used curative therapy for treating CRC hepatic metastases in unresectable CRLMs, inadequate treatment might induce a higher malignant potential and cause recurrent CRC with a worse prognosis⁴⁵. Our study demonstrated, for the first time, the role of HS stress in inducing CRC invasion and progenitor characteristics mediated through Fra-1, a reported oncogene in tumorigenesis and metastasis (**Figure 6E**). Given the crucial role of Fra-1 in CRC metastasis, we speculate that therapeutic intervention of Fra-1 may represent a promising therapeutic strategy for RFA treatment in the near future.

Acknowledgements

We thank Arian Laurence (Freeman Hospital, UK) for manuscript modification work. This work was supported by the State Key Project on Infection Disease of China (Grant No. 2018ZX10723204-003); National Natural Science Foundation of China (Grant No. 81502530, 81874149, 81572427, 81874189).

Conflict of interest statement

No potential conflicts of interest are disclosed.

References

- Bray F, Ferlay J, Soerjomataram I, Siegel RL, Torre LA, Jemal A. Global cancer statistics 2018: GLOBOCAN estimates of incidence and mortality worldwide for 36 cancers in 185 countries. *CA: Cancer J Clin.* 2018; 68: 394-424.
- Ferlay J, Colombet M, Soerjomataram I, Mathers C, Parkin DM, Piñeros M, et al. Estimating the global cancer incidence and mortality in 2018: GLOBOCAN sources and methods. *Int J Cancer.* 2018; 144: 1941-53.
- Manfredi S, Lepage C, Hatem C, Coatmeur O, Faivre J, Bouvier AM. Epidemiology and management of liver metastases from colorectal cancer. *Ann Surg.* 2006; 244: 254-9.
- Moris D, Pawlik TM. Personalized treatment in patients with colorectal liver metastases. *J Surg Res.* 2017; 216: 26-29.
- Stoltz A, Gagnière J, Dupré A, Rivoire M. Radiofrequency ablation for colorectal liver metastases. *J Visc Surg.* 2014; 151(Suppl 1): S33-44.
- McGahan JP, Gu WZ, Brock JM, Tesluk H, Jones CD. Hepatic ablation using bipolar radiofrequency electrocautery. *Acad Radiol.* 1996; 3: 418-22.
- Leen E, Horgan PG. Radiofrequency ablation of colorectal liver metastases. *Surg Oncol.* 2007; 16: 47-51.
- Kikuchi L, Menezes M, Chagas AL, Tani CM, Alencar RS, Diniz MA, et al. Percutaneous radiofrequency ablation for early hepatocellular carcinoma: risk factors for survival. *World J Gastroenterol.* 2014; 20: 1585-93.
- Heerink WJ, Solouki AM, Vliegenthart R, Ruiter SJS, Sieders E, Oudkerk M, et al. The relationship between applied energy and ablation zone volume in patients with hepatocellular carcinoma and colorectal liver metastasis. *Eur Radiol.* 2018; 28: 3228-36.
- Yang WL, Nair DG, Makizumi R, Gallos G, Ye X, Sharma RR, et al. Heat shock protein 70 is induced in mouse human colon tumor xenografts after sublethal radiofrequency ablation. *Ann Surg Oncol.* 2004; 11: 399-406.
- Nadeau SI, Landry J. Mechanisms of activation and regulation of the heat shock-sensitive signaling pathways. In: Csermely P, Vigh L. *Molecular Aspects of the Stress Response: Chaperones, Membranes and Networks.* New York, NY: Springer; 2007: 100-13.
- Tam WL, Lu HH, Buikhuisen J, Soh BS, Lim E, Reinhardt F, et al. Protein kinase C α is a central signaling node and therapeutic target for breast cancer stem cells. *Cancer Cell.* 2013; 24: 347-64.
- Iskit S, Schlicker A, Wessels L, Peeper DS. Fra-1 is a key driver of colon cancer metastasis and a fra-1 classifier predicts disease-free survival. *Oncotarget.* 2015; 6: 43146-61.
- Fidler IJ. The pathogenesis of cancer metastasis: the 'seed and soil' hypothesis revisited. *Nat Rev Cancer.* 2003; 3: 453-8.
- Gupta GP, Massagué J. Cancer metastasis: building a framework. *Cell.* 2006; 127: 679-95.
- Egeblad M, Werb Z. New functions for the matrix metalloproteinases in cancer progression. *Nat Rev Cancer.* 2002; 2: 161-74.
- Park CH, Lee MJ, Ahn J, Kim S, Kim HH, Kim KH, et al. Heat shock-induced matrix metalloproteinase (MMP)-1 and MMP-3 are mediated through ERK and JNK activation and *via* an autocrine interleukin-6 loop. *J Invest Dermatol.* 2004; 123: 1012-9.
- Akita H, Marquardt JU, Durkin ME, Kitade M, Seo D, Conner EA, et al. MYC activates stem-like cell potential in hepatocarcinoma by a p53-dependent mechanism. *Cancer Res.* 2014; 74: 5903-13.
- Celià-Terrassa T, Kang Y. Distinctive properties of metastasis-initiating cells. *Genes Dev.* 2016; 30: 892-908.
- Gao H, Chakraborty G, Zhang ZG, Akalay I, Gadiya M, Gao YQ, et al. Multi-organ site metastatic reactivation mediated by non-canonical discoidin domain receptor 1 signaling. *Cell.* 2016; 166: 47-62.
- Borcherding N, Kusner D, Kolb R, Xie Q, Li W, Yuan F, et al. Paracrine WNT5A signaling inhibits expansion of tumor-initiating cells. *Cancer Res.* 2015; 75: 1972-82.
- Lu YX, Yuan L, Xue XL, Zhou M, Liu Y, Zhang C, et al. Regulation of colorectal carcinoma stemness, growth, and metastasis by an *miR-200c-sox2*-negative feedback loop mechanism. *Clin Cancer Res.* 2014; 20: 2631-42.
- Tominaga K, Shimamura T, Kimura N, Murayama T, Matsubara D, Kanauchi H, et al. Addiction to the IGF2-ID1-IGF2 circuit for maintenance of the breast cancer stem-like cells. *Oncogene.* 2017; 36: 1276-86.
- Reynolds BA, Weiss S. Generation of neurons and astrocytes from isolated cells of the adult mammalian central nervous system. *Science.* 1992; 255: 1707-10.
- Wolf B, Krieg K, Falk C, Breuhahn K, Keppeler H, Biedermann T, et al. Inducing differentiation of premalignant hepatic cells as a novel therapeutic strategy in hepatocarcinoma. *Cancer Res.* 2016; 76: 5550-61.
- Shaw FL, Harrison H, Spence K, Ablett MP, Simoes BM, Farnie G, et al. A detailed mammosphere assay protocol for the quantification of breast stem cell activity. *J Mammary Gland Biol Neoplasia.* 2012; 17: 111-7.
- Yang RC, Jao HC, Huang LJ, Wang SJ, Hsu C. The essential role of PKC α in the protective effect of heat-shock pretreatment on TNF α -induced apoptosis in hepatic epithelial cell line. *Exp Cell Res.* 2004; 296: 276-84.
- Takeuchi H, Bilchik A, Saha S, Turner R, Wiese D, Tanaka M, et al. c-MET expression level in primary colon cancer: a predictor of tumor invasion and lymph node metastases. *Clin Cancer Res.* 2003; 9: 1480-8.
- Liu XD, Newton RC, Scherle PA. Developing c-MET pathway inhibitors for cancer therapy: progress and challenges. *Trends Mol Med.* 2010; 16: 37-45.
- Feliberti EC, Wagman LD. Radiofrequency ablation of liver metastases from colorectal carcinoma. *Cancer Control.* 2006; 13: 48-51.

31. Nielsen K, van Tilborg AAJM, Meijerink MR, Macintosh MO, Zonderhuis BM, de Lange ESM, et al. Incidence and treatment of local site recurrences following rfa of colorectal liver metastases. *World J Surg.* 2013; 37: 1340-7.
 32. Hof J, Wertenbroek MWJLAE, Peeters PMJG, Widder J, Sieders E, de Jong KP. Outcomes after resection and/or radiofrequency ablation for recurrence after treatment of colorectal liver metastases. *Br J Surg.* 2016; 103: 1055-62.
 33. Hocquet A, Aubé C, Rode A, Cartier V, Sutter O, Manichon AF, et al. Comparison of no-touch multi-bipolar vs. Monopolar radiofrequency ablation for small HCC. *J Hepatol.* 2017; 66: 67-74.
 34. Correa-Gallego C, Fong YM, Gonen M, D'Angelica MI, Allen PJ, DeMatteo RP, et al. A retrospective comparison of microwave ablation vs. Radiofrequency ablation for colorectal cancer hepatic metastases. *Ann Surg Oncol.* 2014; 21: 4278-83.
 35. Hammill CW, Billingsley KG, Cassera MA, Wolf RF, Ujiki MB, Hansen PD. Outcome after laparoscopic radiofrequency ablation of technically resectable colorectal liver metastases. *Ann Surg Oncol.* 2011; 18: 1947-54.
 36. Yoshida S, Kornek M, Ikenaga N, Schmelzle M, Masuzaki R, Csizmadia E, et al. Sublethal heat treatment promotes epithelial-mesenchymal transition and enhances the malignant potential of hepatocellular carcinoma. *Hepatology.* 2013; 58: 1667-80.
 37. Makizumi R, Yang WL, Owen RP, Sharma RR, Ravikumar TS. Alteration of drug sensitivity in human colon cancer cells after exposure to heat: implications for liver metastasis therapy using RFA and chemotherapy. *Int J Clin Exp Med.* 2008; 1: 117-29.
 38. Chen HA, Kuo TC, Tseng CF, Ma JT, Yang ST, Yen CJ, et al. Angiotensin-like protein 1 antagonizes MET receptor activity to repress sorafenib resistance and cancer stemness in hepatocellular carcinoma. *Hepatology.* 2016; 64: 1637-51.
 39. Cheng J, Li M, Lv Y. Sublethal heat treatment promotes epithelial-mesenchymal transition and enhances the malignant potential of hepatocellular carcinoma. *Hepatology.* 2014; 59: 1650.
 40. Medema JP. Cancer stem cells: the challenges ahead. *Nat Cell Biol.* 2013; 15: 338-44.
 41. Cheng P, Wang J, Waghmare I, Sartini S, Coviello V, Zhang Z, et al. FOXD1-ALDH1A3 signaling is a determinant for the self-renewal and tumorigenicity of mesenchymal glioma stem cells. *Cancer Res.* 2016; 76: 7219-30.
 42. Samaeekia R, Adorno-Cruz V, Bockhorn J, Chang YF, Huang S, Prat A, et al. miR-206 inhibits stemness and metastasis of breast cancer by targeting MKL1/IL11 pathway. *Clin Cancer Res.* 2017; 23: 1091-103.
 43. Chaffer CL, Weinberg RA. A perspective on cancer cell metastasis. *Science.* 2011; 331: 1559-64.
 44. Golubnitschaja O, Yeghiazaryan K, Stricker H, Trog D, Schild HH, Berliner L. Patients with hepatic breast cancer metastases demonstrate highly specific profiles of matrix metalloproteinases MMP-2 and MMP-9 after SIRT treatment as compared to other primary and secondary liver tumours. *BMC Cancer.* 2016; 16: 357.
 45. Li D, Kang J, Golas BJ, Yeung VW, Madoff DC. Minimally invasive local therapies for liver cancer. *Cancer Biol Med.* 2014; 11: 217-36.
- Cite this article as:** Zhang Z, Zhang Y, Zhang L, Pei Y, Wu Y, Liang H, et al. Incomplete radiofrequency ablation provokes colorectal cancer liver metastases through heat shock response by PKC α /Fra-1 pathway. *Cancer Biol Med.* 2019; 16: 542-55. doi: 10.20892/j.issn.2095-3941.2018.0407

Supplementary materials

Table S1 Total Flux Value of different organs

Liver			Lung			Colon and rectum		
Sham	CR	ICR	Sham	CR	ICR	Sham	CR	ICR
Total Flux (p/s)								
5.28E+06	9.30E+04	9.16E+07	1.50E+04	4.30E+03	9.60E+06	7.50E+04	3.00E+03	5.60E+06
7.26E+06	7.15E+04	1.17E+06	8.00E+03	1.30E+04	1.17E+04	5.80E+04	7.50E+03	1.17E+07
5.59E+06	1.22E+05	7.26E+07	7.00E+03	2.50E+03	6.70E+04	2.67E+05	1.15E+04	7.26E+05
7.99E+06	6.37E+04	1.28E+07	8.00E+03	1.37E+04	1.38E+07	8.00E+03	5.70E+03	1.38E+05
4.53E+07	3.04E+05	1.48E+07	4.00E+03	3.20E+03	5.40E+04	3.40E+04	3.04E+05	9.50E+07
8.72E+06	1.72E+04	9.00E+06	8.00E+03	7.18E+03	9.30E+03	1.80E+04	1.72E+04	9.00E+06
1.41E+07	1.41E+05	4.13E+06	3.00E+04	4.13E+03	1.30E+04	1.41E+06	1.41E+05	7.13E+05
9.69E+06	9.69E+04	5.68E+06	6.00E+03	5.86E+03	8.20E+04	6.00E+03	9.69E+04	5.68E+06
4.71E+06	4.71E+04	8.52E+06	1.20E+04	6.12E+03	8.52E+06	1.20E+04	4.71E+04	8.52E+04
1.32E+07	3.21E+04	1.02E+07	8.90E+03	9.30E+02	1.42E+04	3.10E+04	3.21E+04	1.02E+07
8.72E+06	1.72E+04	9.00E+06	8.30E+03	6.88E+03	8.30E+03	1.80E+04	1.72E+04	9.01E+06
1.41E+07	1.41E+05	4.13E+06	1.41E+04	4.30E+03	4.13E+04	3.12E+04	1.41E+05	4.13E+05
9.69E+06	9.69E+04	5.68E+06	5.30E+03	9.50E+02	7.20E+03	4.78E+03	9.69E+04	5.67E+04
4.71E+06	4.71E+04	8.52E+06	7.20E+03	5.12E+03	6.70E+03	3.20E+04	4.71E+04	4.34E+05
1.32E+07	3.21E+04	1.02E+07	9.13E+02	7.10E+03	2.10E+04	1.13E+04	3.21E+04	1.02E+07

Table S2 Taqman probes used in article

Gene name	Catalog no.
Mmp1a	Mm00473485_m1
Mmp2	Mm00439498_m1
Mmp9	Mm00442991_m1
Mmp3	Mm00440295_m1
Mmp7	Mm00487724_m1
Mmp14	Mm00485054_m1
Mmp20	Mm00600244_m1
Fosl1	Mm04207958_m1
Myc	Mm00487804_m1

Table S3 Antibodies used in article

Antibody name	Vendor	Cat log#
β -actin	Sigma	A5316
Cyclin D1	Santa Cruz	sc8396
Cyclin D2	Cell signaling	3741
Cdk2 (M2)	Santa Cruz	sc163
p-p44/42 (T201/Y204)	Cell signaling	4376
ERK2 (MAPK p42)	Cell signaling	9108
Fra-1 (R-20)	Santa Cruz	sc-605
Phospho-FRA1 (Ser265)	Cell signaling	5841
MMP1	Chemicon	AB8102
Myc (N-262)	Santa Cruz	SC764
p21 (C-19)	Santa Cruz	sc397
p27 Kip1	Cell signaling	3686
Rb	Pharminggen	554136
Phospho-Rb (Ser807/811)	Cell signaling	9308

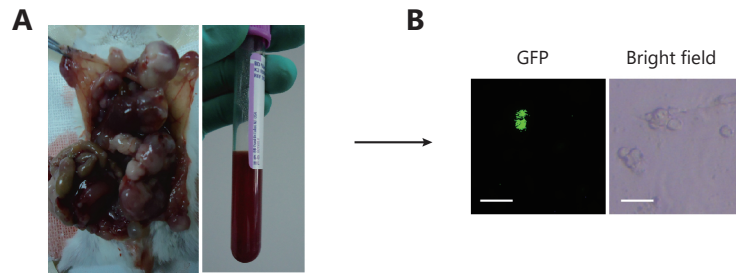


Figure S1 Incomplete ablation induces CRLMs recurrence *in vivo*. (A) Anatomy of a mouse treated by incomplete ablation treatment mouse, metastases were widely observed, and there is about 2ml bloody ascites. (B) GFP positive tumor cells were found in bloody ascites (magnification: 200×).

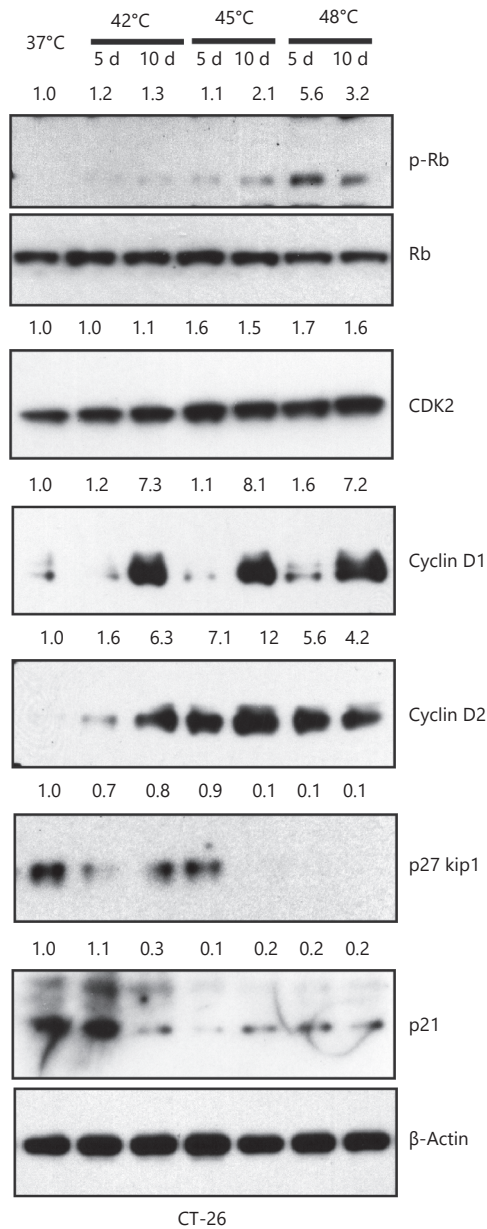


Figure S2 Heat shock promotes tumor-initiating cell traits. Western blot showed the change of cell cycle related protein expression in treated and untreated group in CT-26 cells. The quantification value was labeled above the bands.

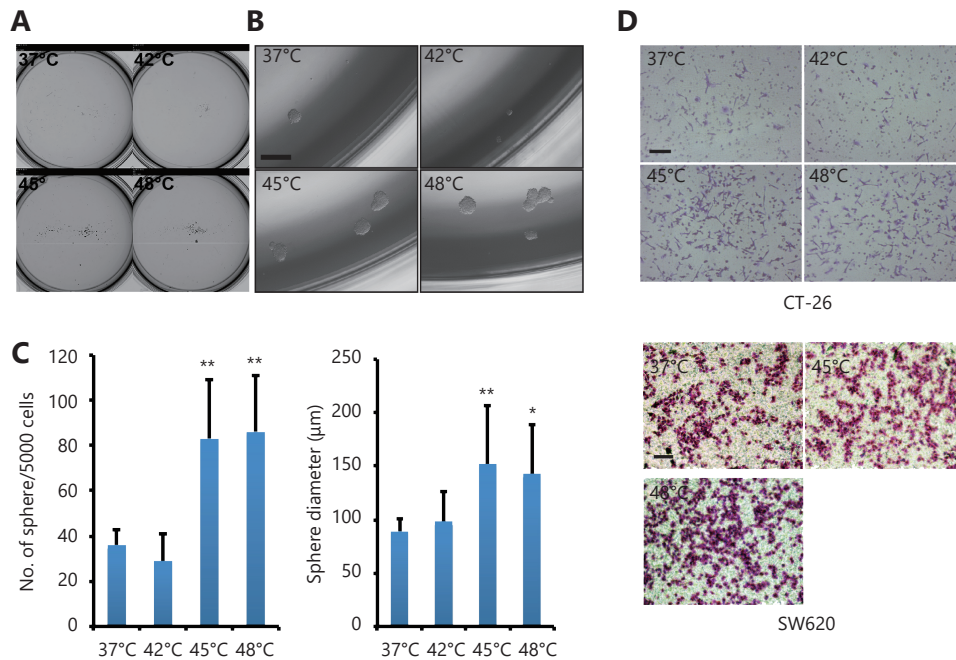


Figure S3 Heat shock promotes tumor-initiating cell traits. (A, B) Phase-contrast pictures of tumor spheres formed by pre-heat shock treated SW620 cells, grown in serum-free sphere medium on Ultra-low attachment surface plates. Whole view of sphere assay was showed in panel A, representative magnified view was showed in B. scale bar, 50 μm. (C) Quantification of tumor spheres formed by SW620 cells. The mean number of spheres per 5000 cells and the mean diameter of spheres are calculated in triplicate samples, * $P < 0.05$, ** $P < 0.01$. (D) Representative images of matrigel pre-coated transwell assays with CT-26 and SW620 cells.

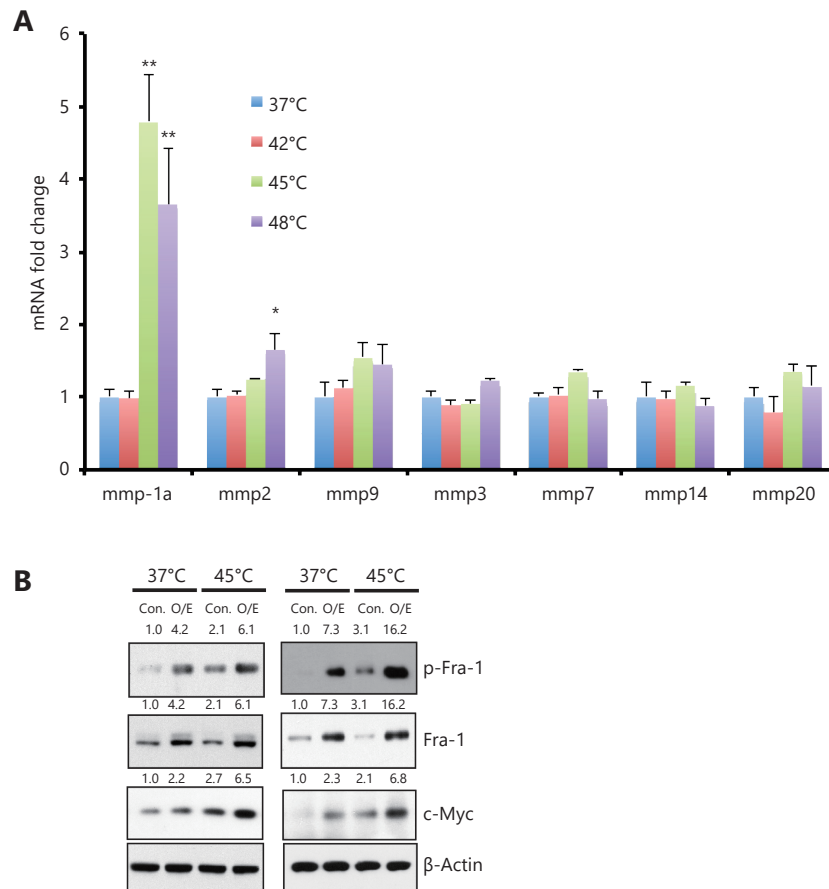


Figure S4 Heat shock up-regulated MMP1 expression. (A) *Mmps* mRNA level in CT-26 cells, which was qualified by qPCR assay. Mmp1a is a representative member of Collagenases, Mmp2 and Mmp9 are belong to Gelatinases, MMP3 is one of Stromelysins, MMP7 is one of Matrilysin, Mmp14 is a membrane-type MMPs, and MMP20 belong to Enamelysin. Western Blot assay showed over expression of Fra-1 induced c-Myc expression. (B) The quantification value was labeled above the bands.

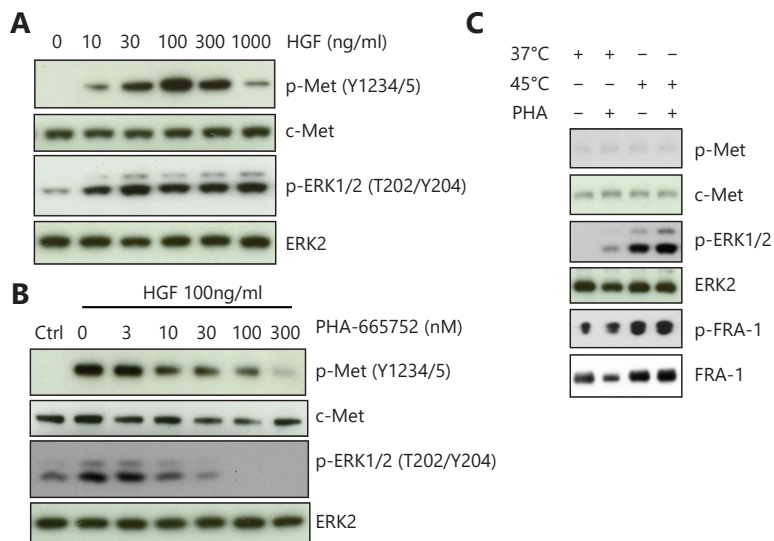


Figure S5 The induction of ERK1/2 and Fra-1 phosphorylation by heat shock is independent of c-Met activation. (A) Western blot assay showed HGF induced c-Met and downstream ERK phosphorylation in a dose-dependent manner. (B) c-Met inhibitor PHA-665752 blocked HGF induced c-Met and ERK phosphorylation in a dose-dependent manner. (C) Western blot assay showed c-Met was not phosphorylated by heat shock, even though downstream ERK was activated. Furthermore, c-Met inhibitor PHA-665752 cannot block the ERK and Fra-1 phosphorylation induced by 45°C heat shock in CT-26 cells.

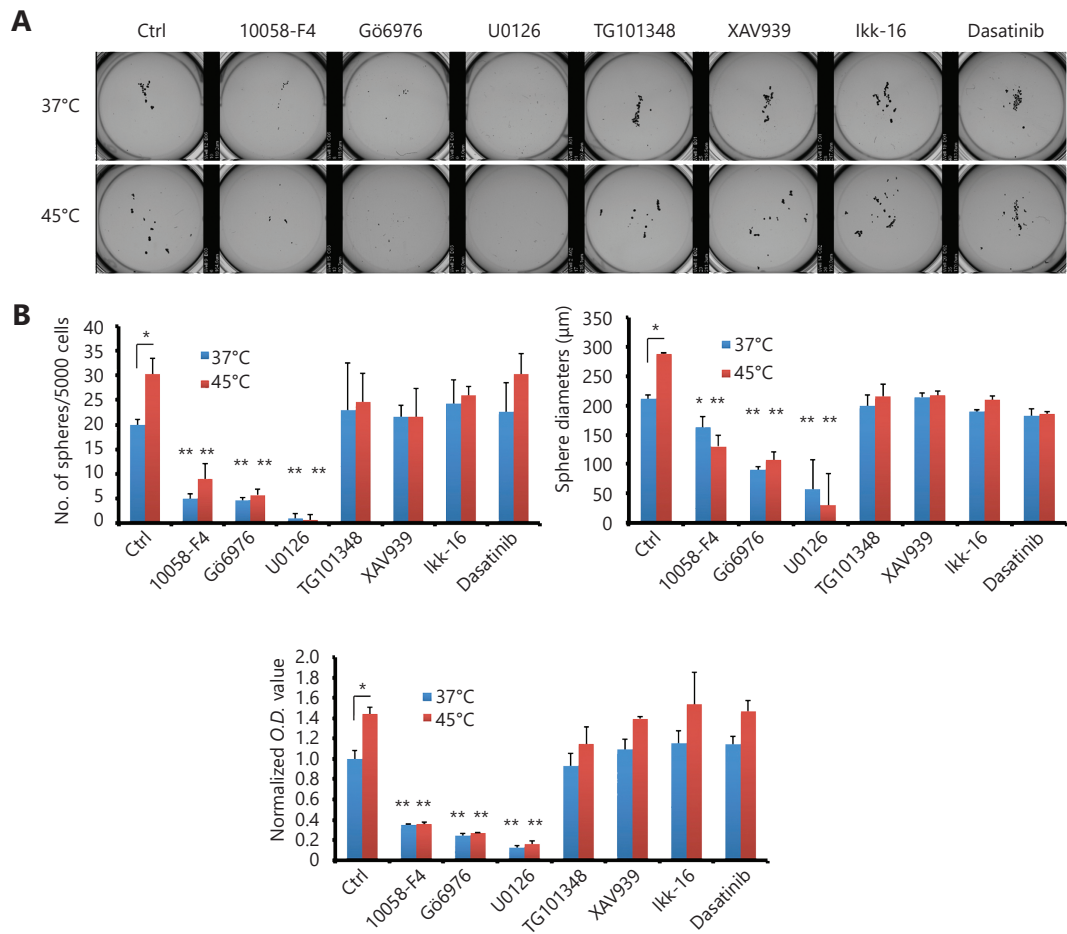


Figure S6 Inhibition of PKC α -ERK1/2-Fra-1 signaling abolished the heat shock-induced malignant effects. (A) Sphere-forming assay of CT-26 cells treated with or without HS and with a panel of different inhibitors, 10058-F4 (500 nM), Gö6976 (500 nM), U0126 (5 μ M), TG101348 (500 nM), XAV939 (500 nM), Ikk-16 (500 nM) and Dasatinib (500 nM). Representative whole view images of spheres are shown. (B) Quantification of the spheres by Gel count machine and MTT assay. * $P < 0.05$, ** $P < 0.01$. $n = 3$.